Optical and Quantum Electronics (2018) 50:406
https://doi.org/10.1007/s11082-018-1667-x

Vortex dynamics of counterpropagting laser beams in photorefractive materials

Mihailo Čubrović[1] · **Milan Petrović**[2,3]

Received: 13 October 2017 / Accepted: 12 October 2018

Abstract
We study vortex patterns of counterpropagating laser beams in a photorefractive crystal, with or without the background photonic lattice. The vortices are effectively planar and have two "flavors" because there are two opposite directions of beam propagation. In a certain parameter range, the vortices form stable equilibrium configurations which we study using the methods of statistical field theory and generalize the Berezinsky–Kosterlitz–Thouless transition of the XY model to the "two-flavor" case. In the nonequilibrium regime, the patterns exhibit an Andronov–Hopf bifurcation which may lead to oscillations (limit cycle), chaos or decay to zero intensity due to radiation losses. We show how to identify various pathways toward instability from intensity patterns, i.e. from experiment.

Keywords Vortex · BKT transition · Photorefractive optics · Statistical field theory

1 Introduction

Nonlinear optical systems are a rich arena for studies of various fundamental physical phenomena. The strong response of the nonlinear optical medium to the propagation of light makes it a typical strongly correlated system, with many phenomena similar to those in other strongly interacting systems in areas such as condensed matter. Their complex dynamics offers an opportunity to study spatiotemporal chaos and optical turbulence

This article is part of the Topical Collection on Focus on Optics and Bio-photonics, Photonica 2017.

Guest Edited by Jelena Radovanovic, Aleksandar Krmpot, Marina Lekic, Trevor Benson, Mauro Pereira, Marian Marciniak.

✉ Mihailo Čubrović
mcubrovic@gmail.com

Milan Petrović
petrovic@ipb.ac.rs

[1] Scientific Computing Laboratory, Institute of Physics, University of Belgrade, Pregrevica 118, Belgrade 11080, Serbia

[2] Institute of Physics, P. O. B. 57, Belgrade 11001, Serbia

[3] Texas A&M University at Qatar, Doha P.O.Box 23874, Qatar

Published online: 26 October 2018

(Cross and Hohenberg 1993; Rabinovich et al. 2000). On the other hand, they often also exhibit stable, equilibrium confgurations in a certain parameter range, which are nautrally studied by statistical physics methods. Vortices and other topological configurations (Alexander et al. 2007; Anderson 2007; Fetter 2009), long-range order (Anderson 2007), quenched disorder and glassy behavior (Antenucci et al. 2015a, b; Ghofraniha 2015; Perret et al. 2012) are universal in a broad range of systems such as cold atoms (Bagnato et al. 2015; Malomed et al. 2016) and magnetic systems, and the relative simplicity of experiments in optics makes it an excellent testing ground for strongly coupled models.

In this paper we study a specific and experimentally realizable nonlinear optical system: laser beams counterpropagating (CP) through a photorefractive (PR) crystal. This means we have an elongated PR crystal (with one longitudinal and two transverse dimensions) and two laser beams shone onto each end. We thus effectively have two fields, one forward-propagating and one backward-propagating. The optical response of the crystal depends nonlinearly on the *total* intensity of both beams, which means the beams effectively interact with each other. This system has been thoroughly investigated for phenomena such as dynamical solitons (Denz et al. 2003; Petrović et al. 2011, 2005; Jović et al. 2008), vortex stability on the photonic lattice (Alexander et al. 2007; Terhalle et al. 2008; Čubrović and Petrović 2017) and topological invariants (Rechtsman et al. 2013).

We first recast the system in Lagrangian and then in Hamiltonian form so it can be studied as a field theory, which depends parametrically on the time t. Then we consider the time dynamics of the system and show that in a broad parameter range the patterns relax to a static configuration which can be studied within *equilibrium* field theory. By renormalization group (RG) analysis, we obtain the phase diagram of static vortex configurations. The phase diagram is obviously closely related to the famous Berezinsky–Kosterlitz–Thouless (BKT) vortex unbinding transition in the XY model (Berezinsky 1971; Kosterlitz and Thouless 1973) except that having two components of the field produces additional phases and phase transitions, due to forward–backward beam interaction. The analytical insight we obtain also allows us to avoid overextensive numerics – analytical construction of the phase diagram tells us which patterns can in principle be expected in different corners of the parameter space.

Next we focus on the nonequilibrium regime, classify the fixed points and study possible routes of instability. We emphasize the pictorial and "rule-of-thumb" criteria to recognize various instabilities, in order to facilitate experimental checks. At the end we will discuss the perspective of studying dynamical criticality, i.e. instablities which consist in moving from one vortex phase to another in real time, a phenomenon which is intimately connected to the difficult questions of quench dynamics and thermalization in many-body systems.

2 Counterpropagating beams in photorefractive medium: equations of motion

Consider a photorefractive crystal of length L irradiated by two paraxial head-on laser beams which propagate from the opposite faces of the crystal in the z-direction. Photorefractive crystals induce self-focusing of the beams—the vacuum (linear) wave equation is modified by the addition of a friction-like term, so the diffusion of the light intensity (the broadening of the beam) is balanced out by the self-focusing of the beam. The physical ground for this is the redistribution of the charges in the crystal due to the Kerr effect.

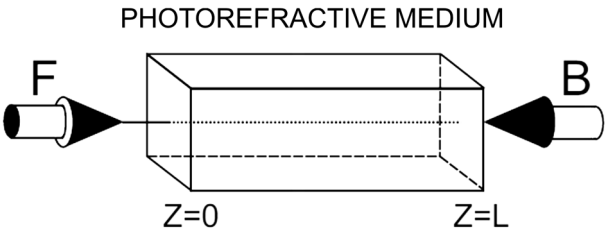

Fig. 1 Experimental setup for the study of the CP beams in the PR crystal. The crystal has the shape of a parallelepiped, and the beams propagate along the longitudinal, z-axis: the forward (F)-beam from $z = 0$ to $z = L$, and the backward (B)-beam the other way round. The intensity patterns can be observed at the transverse faces of the crystal, at $z = 0$ and $z = L$

The nonlinearity is contained in the change of the refraction index which is determined by the induced charge density. A sketch of the system is given in Fig. 1. Before entering the crystal, the laser beams can be given any desirable pattern of both intensity and phase. In particular, one can create vortices (winding of the phase) making use of the phase masks (Denz et al. 2003).

Assuming the electromagnetic field of the form $\mathbf{E} = e^{\imath\omega t+\imath\mathbf{qr}}\left(Fe^{ikz} + Be^{-ikz}\right)$, we can write equations for the so-called envelopes F and B of the forward- and backward-propagating beams along the z-axis (the frequency, transverse and longitudinal momentum are denoted respectively by $\omega, \mathbf{q}, k$). The wave equations for F and B are now:

$$\pm\imath\partial_z\Psi_\pm(z;x,y;t) + \Delta\Psi_\pm(z;x,y;t) = \Gamma E(z;x,y;t)\Psi_\pm(z;x,y;t), \tag{1}$$

where the plus and minus signs on the left-hand side stand for the forward- and backward-propagating component of the beam amplitude doublet $\Psi \equiv (\Psi_+, \Psi_-) \equiv (F, B)$, and Γ is the dimensionless PR coupling constant. From now on we will use $\alpha \in \{+, -\}$ to denote the two beams (F and B) and call it a flavor index, in analogy with field theory. The vorticity (winding number of the phase) will be called vortex charge as usual. The charge field E on the right-hand side of the equation is the electric field sourced by the charges in the crystal (i.e., it does not include the external electric field of the beams). Its evolution is well represented by a relaxation-type equation (notice that the derivative ∂_E is strictly negative) (Petrović et al. 2011):

$$\frac{\tau}{1 + I(z;x,y;t)}\partial_t E(z;x,y;t) + E(z;x,y;t) = -\frac{I(z;x,y;t)}{1 + I(z;x,y;t)}. \tag{2}$$

Here, $I \equiv I_\Psi + I_x$ is the total light intensity at a given point, $I_\Psi \equiv |F|^2 + |B|^2$ is the beam intensity and I_x the intensity of the fixed background. The meaning of I_x is that the crystal is all the time irradiated by some constant light source, independent of the counterpropagating beams with envelopes F, B. The relaxation time is τ. The form of the nonlinearity accounts for the saturation of the crystal; notice that a simple quartic non-linear Schrödinger equation would not account for the saturation.[1] In the numerical calculations,

[1] One might also worry that a realistic crystal is anisotropic, while our equation is isotropic. Nevertheless, comparison to experiment (Neshev et al. 2004; Fleischer et al. 2004; Dreischuh et al. 2002) shows that this model is able to describe actual measurements rather well. Also, the effects of anisotropy can be suppressed in experiment by illuminating the crystal by *uniform* light for very long times before starting the experiment (Cohen et al. 2002).

we solve Eqs. (1), (2) with no further assumptions, using a slightly modified version of the beam propagation method (Sandfuchs et al. 2001). For analytical results we will need to transform them further assuming a vortex pattern. The Eq. (2) is completely phenomenological, but it excellently represents the experimental results (Denz et al. 2003). We will first consider the equilibrium regime, and then the nonequilibrium dynamics.

For slow time evolution (in absence of pulses), we can Laplace-transform the Eq. (2) in time ($E(t) \mapsto E(u) = \int_0^\infty dt e^{-ut} E(t)$) to get the algebraic relation

$$E(z;x,y;u) = -\frac{\Psi^\dagger\Psi + I_x - \tau E_0}{1 + \tau u + I_x + \Psi^\dagger\Psi} = -1 + \frac{1 + \tau u + \tau E_0}{1 + \tau u + I_x + \Psi^\dagger\Psi}. \tag{3}$$

The original system (1) can now be described by the Lagrangian:

$$\mathcal{L} = \imath\Psi^\dagger\sigma_3\partial_z\Psi - |\nabla\Psi|^2 + \Gamma\Psi^\dagger\Psi - \Gamma(1 + \tau E_0 + \tau u)\log(1 + \tau u + I_x + \Psi^\dagger\Psi), \tag{4}$$

where σ_3 is the Pauli matrix $\sigma_3 = \mathrm{diag}(1,-1)$. This has the form $\mathcal{L} = \imath\Psi^\dagger\sigma_3\partial_z\Psi - |\nabla\Psi|^2 - V_{eff}(\Psi^\dagger,\Psi)$, i.e. the Lagrangian of a non-relativistic field theory (a two-component nonlinear Schrödinger field equation) in $2+1$ dimensions (x, y; z), where the role of time is played by the longitudinal distance z, and the physical time t (or u upon the Laplace transform) is a parameter.

3 Stable vortex configurations and the phase diagram

Following the same steps as for the textbook XY model we can arrive at an effective Hamiltonian for stable vortex configurations. For details we refer the reader to Čubrović and Petrović (2017). Assuming the vortex solution of the form

$$\Psi_{0\pm}(\mathbf{r}) = \psi_{0\pm}(r)e^{\imath\delta\theta_\pm(\phi)+\imath\theta_{0\pm}(\phi)}, \tag{5}$$

where $\theta_\pm(\phi)$ is the singular part of the phase and $\theta_{0\pm}(\phi)$ the regular part, we want to integrate out both the amplitude fluctuations and the regular part of the phase and arrive at a description of the systems solely in terms of vortex charges. This is done by expanding the Lagrangian (4) to quadratic order in both amplitude and phase fluctuations and integrating them out. Then the usual Legendre transform yields the vortex Hamiltonian:

$$\mathcal{H}_{\mathrm{vort}} = \sum_{i<j}\left(gQ_{i\alpha}Q_{j\alpha} + g'Q_{i\alpha}\times Q_{j\beta}\right)\log r_{ij} + \sum_i\left(g_0Q_{i\alpha}Q_{i\alpha} + g_1Q_{i\alpha}\times Q_{i\beta}\right). \tag{6}$$

We denote the flavor $\pm$ by Greek indices, and the summation convention is understood.[2] Furthermore, we denote $Q_\alpha \times Q_\beta \equiv Q_{i+}Q_{j-} + Q_{i-}Q_{j+}$. The first term is the expected Coulomb interaction of vortices from the XY model (Berezinsky 1971; Kosterlitz and Thouless 1973); notice that only like-flavored charges interact through this term (because the kinetic term $|\nabla\Psi|^2$ is homogenous quadratic). The second term is the forward–backward interaction, also with Coulomb-like (logarithmic) radial dependence. This interaction is generated by the coupling of amplitude fluctuations $\delta\psi_\alpha(r)$ to the phase fluctuations. In a system without amplitude fluctuations, i.e. classical spin system, this term would not be generated. The third and fourth term constitute the energy of the vortex core. The self-interaction

[2] There is no difference between upper and lower indices as both flavors always enter the sum with positive sign.

constants g_0, g_1 are of course dependent on the vortex core size and behave roughly as $g \log a/\epsilon, g' \log a/\epsilon$, where ϵ is the UV cutoff. The final results will not depend on ϵ, as expected, since g_0, g_1 can be absorbed in the fugacity y (see the next subsection). Expressions for the coupling constants in terms of original parameters are given in Čubrović and Petrović (2017); they can be used to relate the theoretical phase diagram to experiment.

To describe the phase diagram, we will perform the renormalization group (RG) analysis. Here we follow closely the calculation for conventional vortex systems. We consider the fluctuation of the partition function $\delta\mathcal{Z}$ upon the formation of a virtual vortex pair at positions $\mathbf{r}_1, \mathbf{r}_2$[3] with charges $q_\alpha, -q_\alpha$, (with $\mathbf{r}_1 + \mathbf{r}_2 = 2\mathbf{r}$ and $\mathbf{r}_1 - \mathbf{r}_2 = \mathbf{r}_{12}$), in the background of a vortex pair at positions $\mathbf{R}_1, \mathbf{R}_2$ (with $\mathbf{R}_1 + \mathbf{R}_2 = 2\mathbf{R}$ and $\mathbf{R}_1 - \mathbf{R}_2 = \mathbf{R}_{12}$) with charges $Q_{1\alpha}, Q_{2\alpha}$. It is also convenient to replace the core self-interaction constants $g_{0,1}$ with the fugacity parameter defined as $y \equiv \exp\left[-\beta\left(g_0 + g_1\right)\log\epsilon\right]$. We also introduce the notation $\beta \equiv L$ in analogy with the inverse temperature β in standard statistical mechanics but of course the physical meaning of β in our system is very different: we have no thermodynamic temperature or thermal noise, and the third law of thermodynamics is not satisfied for the "temperature" $1/\beta$. We merely use the β-notation for reasons of formal similarity, not as a complete physical analogy.

This is a straightforward but lengthy calculation and we state just the resulting flow equations:

$$\frac{\partial g}{\partial \ell} = -16\pi(g^2 + g'^2)y^4, \quad \frac{\partial g'}{\partial \ell} = -2\pi g g' y^4, \quad \frac{\partial y}{\partial \ell} = 2\pi(1 - g - g')y. \tag{7}$$

Notice that if one puts $g' = 0$, they look very much like the textbook XY model RG flow, except that the fugacity enters as y^4 instead of y^2 (simply because every vortex contributes two charges). We can find fixed points analytically and then numerically integrate the flow equations to find exact phase borders. The fugacity y can flow to zero (meaning that the vortex creation is suppressed and the vortices tend to bind) or to infinity, meaning that vortices can exist at finite density. At $y = 0$ there is a fixed line $g + g' = 1$. This line is attracting for the half-plane $g + g' > 1$; otherwise, it is repelling. There are three more attraction regions when $g + g' < 1$. First, there is the point $y \to \infty, g = g' = 0$ which has no analogue in single-component vortex systems. Then, there are two regions when $g \to \infty$ and $g' \to \pm\infty$ (and again $y \to \infty$). Of course, the large g, g' regime is strongly interacting and the perturbation theory eventually breaks down. What happens when g, g' flow toward very large values is that the intensity at the vortex core becomes very large, so the lowest-order, quadratic Hamiltonian needs to be supplemented by higher-order terms in intensity fluctuations. To integrate them out, one needs to perform a diagrammatic expansion which leads to quartic- and higher-order terms in vortex charges Q_α in the effective vortex Hamiltonian [Eq. (6)], ultimately correcting the flow at large g, g' to flow toward finite values g_*, g'_* and g_{**}, g'_{**}.

The RG flows in the $g - g'$ plane are given in Fig. 2. The situation is now the following:

1. The attraction region of the fixed line is the vortex insulator phase (INS): the creation rate of the vortices is suppressed to zero. There is no vortex charge conservation.

[3] The boldface vectors are the coordinate vectors in the plane.

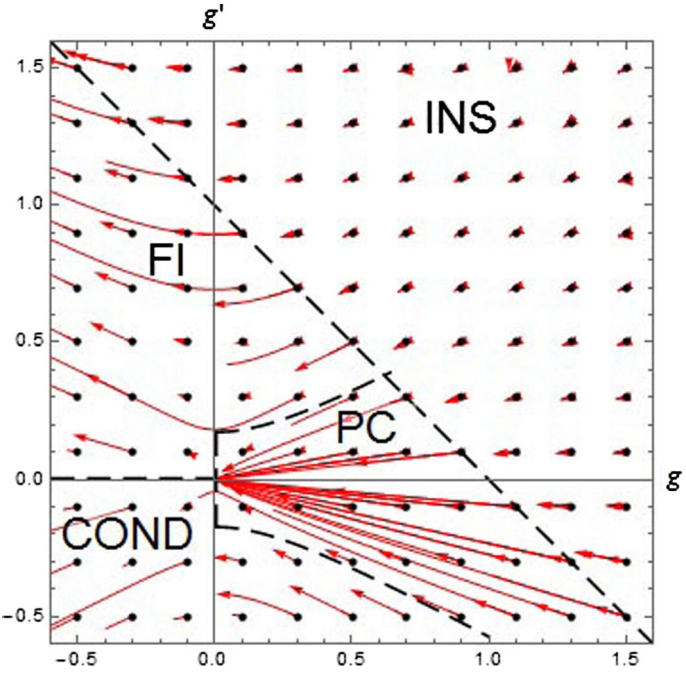

Fig. 2 Phase diagram for the clean system in the $g-g'$ plane, at the mean-field level with RG flows. We show the flows for a grid of initial points, denoted by black dots; red lines are the flows. Four phases exist, whose boundaries are delineated by black dashed lines: conductor (COND), insulator (INS), frustrated insulator (FI) and perfect conductor (PC). The straight line $g + g' = 1$ is obtained analytically whereas the other phase boundaries can only be found by numerical integration of the flow Eq. (7). The flows going to infinity are the artifacts of the perturbative RG; they correspond to finite values which are beyond the scope of our analytical approach. Notice how the flows in the $g + g' > 1$ phase all terminate at different values

2. The zero-coupling fixed point attracts the trajectories in the vortex perfect conductor phase (PC): only the fugacity controls the vortices and arbitrary charge configurations can form. Each vortex charge, Q_+ and Q_-, is separately conserved.
3. In the attraction region of the fixed point with $g_* < 0$ and $g'_* > 0$ (formally they flow to $-\infty$ and $+\infty$, respectively), same-sign F- and B-charges attract each other and those with the opposite sign which repel each other. This is the frustrated insulator (FI): it conserves only the combination $Q_+ + Q_-$, and only vortices with charge $(Q_+, -Q_+)$ are stable.
4. The fixed point with $g_{**}, g'_{**} < 0$ (formally both flow to $-\infty$) corresponds to the conductor phase (COND). This phase preserves one of the charges, Q_+ or Q_-, i.e. either $(Q_+, 0)$- or $(0, Q_-)$-vortices proliferate.

In the half-plane $g + g' > 1$ every point evolves toward a different, finite point (g, g') in the same half-plane. In the other half-plane we see the regions of points moving toward the origin or toward one of the two directions at infinity. In the future we plan to apply this formalism also to multi-component vortices in Bose–Einstein condensates (Ma et al. 2016) and in particular in type-1.5 superconductors (Silaev and Babev 2012), where even more complex phenomena, including frustration, are observed as a consequence of multi-component interaction.

An interesting line of research consists in adding disorder to the above system. We consider this problem in Čubrović and Petrović (2017) and find that the system can be approximated by a random-coupling *and* random-field two-component XY-like model, related to the Cardy–Ostlund model (1982). The replica formalism (Castellana and Parisi 2015) then predicts a glassy phase with slow dynamics, strong correlations and no long-range order. This is however a separate story and we will leave it out here. Interested readers can consult (Čubrović and Petrović 2017) and look at related work in Antenucci et al. (2015a, b).

4 Time-dependent regime

Here our goal is twofols. First, we have to show that at least for some boundary conditions and parameter values there is a stable fixed point of the time evolution, so that the system reaches a time-independent, equilibrium pattern. The reason is that the whole formalism of the previous chapter is only valid for such configurations, as it departs from equilibrium statistical mechanics. Second, we want to check other, non-static behaviors as they are interesting in their own right and experimentally relevant (but one should not expect them to be described by an equilibrium phase diagram like Fig. 2).

Time dynamics can be studied in a straightforward way, making use of the relaxation Eq. (2) to write down the first-order evolution equations for $\Psi_\pm$:

$$\frac{\partial \Psi_\alpha^\pm}{\partial t} = -\frac{\Gamma}{\tau}\frac{((1+I)E+I)}{\alpha k - q^2 - \Gamma E}\Psi_\alpha^\pm, \quad \frac{\partial E}{\partial t} = -\frac{1}{\tau}((1+I)E+I). \tag{8}$$

This system has three equilibrium points. One is the trivial equilibrium with zero intensity ("0" point):

$$\left(\Psi_+^\pm, \Psi_-^\pm, E\right) = \left(0, 0, -\frac{I_x}{1+I_x}\right),$$

and the remaining two are related by a discrete symmetry $\Psi_\pm \mapsto \Psi_\mp$ ("$\pm$" points). The "+" point is

$$\left(\Psi_+^\pm, \Psi_-^\pm, E\right) = \left(\sqrt{\frac{E(1+I_x)+I_x}{1+E}}e^{\imath\phi_+}, 0, E\right),$$

and the "−" point has instead $\Psi_+ = 0$ and $\Psi_- = \sqrt{(E(1+I_x)+I_x)/(1+E)}\exp(\imath\phi_-)$. Notice that the phase $\phi_\pm$ remains free to vary so the "$\pm$" solutions support vortices. We first ask what is the stability criterion for a nontrivial solution, i.e. one of the "$\pm$" points, as this is the main criterion for the applicability of the equilibrium statistical mechanics methods in the previous section. Introducing the amplitudes of the fluctuations from equilibrium as $X_{1,3} = \Re\delta\Psi_\pm, X_{2,4} = \Im\delta\Psi_\pm, X_5 = \delta E$, we can do a first-order stability analysis as the system is non-degenerate. Rescaling $X_1 \mapsto (1+E_0)^{-3/4}\left(I_x + E_0\left(1+I_x\right)\right)^{1/2}$ and $t \mapsto t\left(\left(1+E_0\right)/\left(I_x + E_0\left(1+I_x\right)\right)\right)^{1/4}$, the equation of motion for the "$\pm$" point reads

$$\partial_t\begin{pmatrix}X_1\\X_5\end{pmatrix} = \begin{pmatrix}-\frac{a_\pm}{\Gamma E_0+k+q^2} & -1\\ 1 & -\frac{a_\pm}{\Gamma E_0+k+q^2}\end{pmatrix}\begin{pmatrix}X_1\\X_5\end{pmatrix} + O(X_1^2+X_5^2; X_2, X_3, X_4), \tag{9}$$

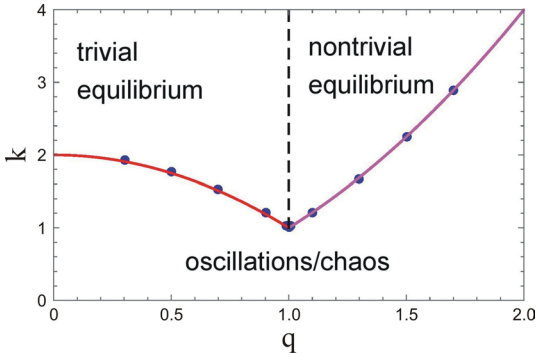

Fig. 3 Stability diagram in the q–k plane. The onset of instability for $k < k_c(q)$ is found numerically for a range of q values. The solid lines are the analytical prediction for the stability of the "0" point ($k_c = q^2$, magenta) and of the "+" point ($k_c = \Gamma E_0 - q^2 \approx \Gamma - q^2$, red). The black dashed line at $q = q_c \approx 1$ separates the stability regions of the two points. The domain of applicability of our main results is the top right corner (nontrivial equilibrium), above $k > k_{\min} \sim 1/L$ and for not too large q values. Parameter values: $\Gamma = 2, I_x = 0$

with $a_\pm$ being some (known) *positive* functions of Γ, E_0, I_x (independent of k, q). This is precisely the normal form for the Andronov–Hopf bifurcation (Arnol'd et al. 1994), and the bifurcation point lies at $k = -\Gamma E_0 - q^2$. To remind, the bifurcation happens when the off-diagonal element in the linear term changes sign: the fixed point is stable when $a_\pm/(\Gamma E_0 + k + q^2)$ is positive. The sign of the nonlinear term determines the supercritical/subcritical nature of the bifurcation.[4]

Now the textbook analysis of the Andronov–Hopf bifurcation tells us that stable "+" equilibrium exists for $k > -\Gamma E_0 - q^2$ where E_0 is best found numerically. Exactly the same condition holds for the "−" point. For $k < -\Gamma E_0 + q^2$, dynamics depends on the sign of the nonlinear term in Eq. (9). For the positive sign we expect periodically changing patterns and for the negative sign (subcritical bifurcation), various possibilities arise: the system may wander chaotically between the "+" and the "−" points, or it may end up in the attraction region of the "0" point and fall onto the trivial solution with zero intensity. Naively, the attraction regions of the two fixed points ("±" and "0") are separated by the condition $-\Gamma E_0 - q^2 = q^2$, i.e. $q_c = \sqrt{-\Gamma E_0(\Gamma, \tau)/2}$, where we have emphasized that E_0 is in general non-universal. The actual boundary may be more complex however, as our analysis is based on finite-order expansion around the fixed points, which is not valid far away from them.

The numerical stability diagram is given in Fig. 3. The stability limit turns out to be $k > \Gamma - q^2$, i.e. $E_0 \approx -1$. The curves separating the attraction regions of the three equilibrium points follow exactly the quadratic scaling in q as predicted by the analytical stability analysis. The equilibrium region lies in the top right corner of the diagram (nontrivial equilibrium), above $k \approx 1/L$. This is where the patterns evolve towards static

[4] Negative sign means the fixed point is stable everywhere before the bifurcation and is replaced by a stable limit cycle after the bifurcation (supercritical). Positive sign means the fixed point coexists with the stable limit cycle before the bifurcation and the (X_1, X_5) plane is divided among their attraction regions; after the bifurcation there is no stable solution at all (subcritical). However, one should not take the stability in the whole (X_1, X_5) plane in the supercritical case too seriously. We have expand the equations of motion in the vicinity of the fixed points and the expansion ceases to be valid far away from the origin.

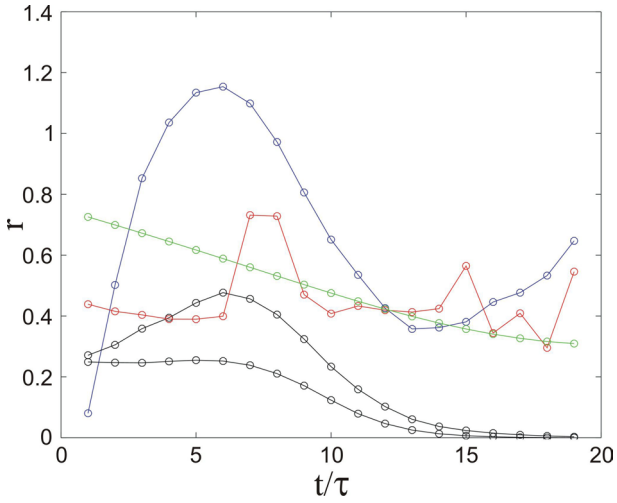

Fig. 4 Time evolution of the relaxation rate r for the various situations from Figs. 5 and 6, illustrating the relaxation to non-trivial (non-zero intensity) equilibrium, i.e. "±" fixed points (Fig. 5a, c, black), limit cycle (6a, blue), chaos (6b, red) and the relaxation to trivial (zero intensity) equilibrium, i.e. "0" fixed point (6c, green). In the main text we mainly study the cases like the black curves, where time-independent stable configurations are seen. The circles are data points from numerics and the lines are just to guide the eye

long-time configurations. The top left corner describes "boring" situations, when all light ultimately radiates away from the crystal and intensity drops to zero. The bottom region contains nontrivial dynamics: depending on parameters, it may contain a limit cycle (correspinding to oscillating patterns) or aperiodic wandering among an alphabet of unstable patterns (chaos).

Formally, both k and q can be any real numbers. In practice, however, k is discrete and its minimal value is of the order $1 / L$. The spatial momentum q lies between the inverse of the transverse length of the crystal (which is typically an order of magnitude smaller than L, i.e. minimal q can be assumed equal to zero) and some typical small-scale cutoff which in our case is the vortex core size.

Now we test our conclusions numerically. A convenient quantity to differentiate between different stability regimes is the relaxation rate

$$r \equiv \frac{1}{X}\frac{dX}{dt} = \frac{\sum_{x,y} |X(t_{j+1};x,y) - X(t_j;x,y)|^2}{\sum_{x,y} |X(t_j;x,y)|^2}, \tag{10}$$

which is expected to reach zero for a generic relaxation process, where in the vicinity of an asymptotically stable fixed point $X \sim X_{\mathrm{eq}} + xe^{-rt}$ will be generically nonzero for a limit cycle or chaos, and will asymptote to a constant for the "0" point, where $X_{\mathrm{eq}} = 0$ so we get $(1/X)dX/dt \sim r$.

Figure 4 summarizes these possibilities in terms of the relaxation rate r, whereas Figs. 5 and 6 show how the patterns evolve in some representative cases. The black curves in Fig. 4 show the situation which is in the focus of this work – the approach toward static equilibrium. This corresponds to the phases from Fig. 2. In Fig. 5 we see how the equilibrium configurations are reached (for three phases). In each case we start with a regular lattice of circular vortices. In the PC phase (Fig. 5a) the vortices expand somewhat but in principle retain the original configuration (and charges). The other two phases (Fig. 5b, c) have nontrivial transient dynamics and undergo the lattice inversion, but eventually (for times about $t \approx 20 - 25\tau$) they stabilize and form a static inverse lattice (with charges $(3, -3)$ in the FI case and with zero charge in the INS case).

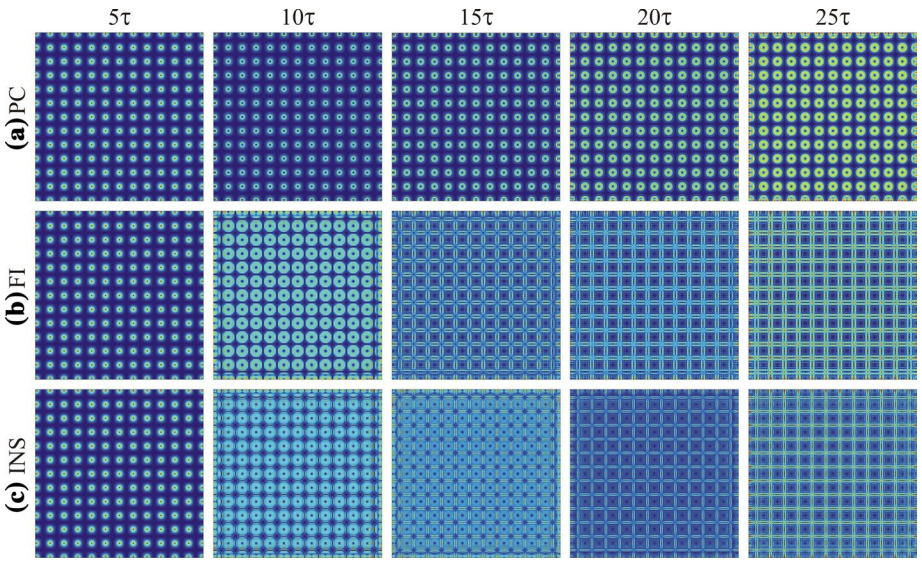

Fig. 5 Time evolution of patterns at five different times: **a** perfect conductor phase, **b** frustrated insulator phase and **c** insulator phase. In all cases the approach to equilibrium is obvious, and we expect that for long times a thermodynamic description is justified

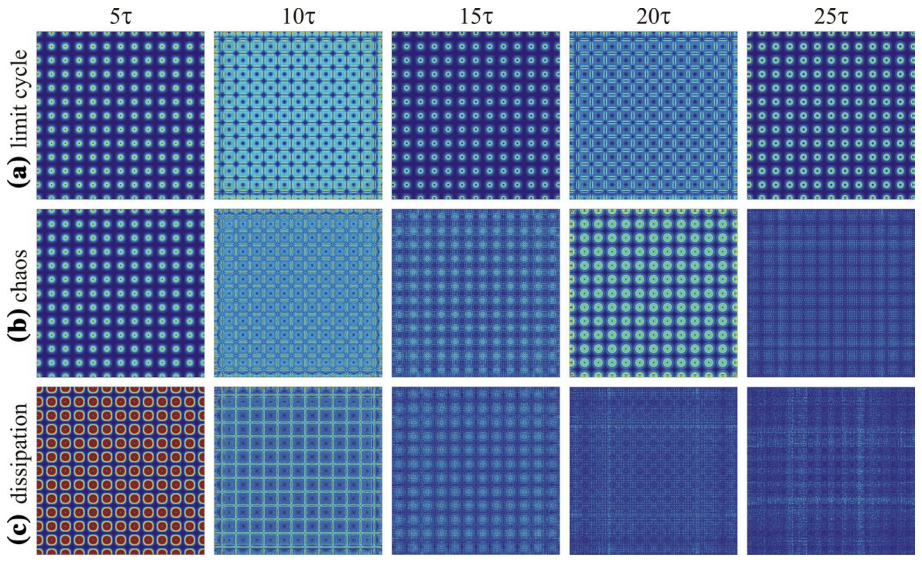

Fig. 6 Time evolution of non-equilibrium patterns. In **a** the limit cycle leads to permanent oscillatory behavior, in **b** wandering along the unstable manifold between the equilibrium points gives rise to chaos and in **c** dissipation wins and dynamics dies out. The parameters are the same as in the previous figure, except that the length L is increased thrice

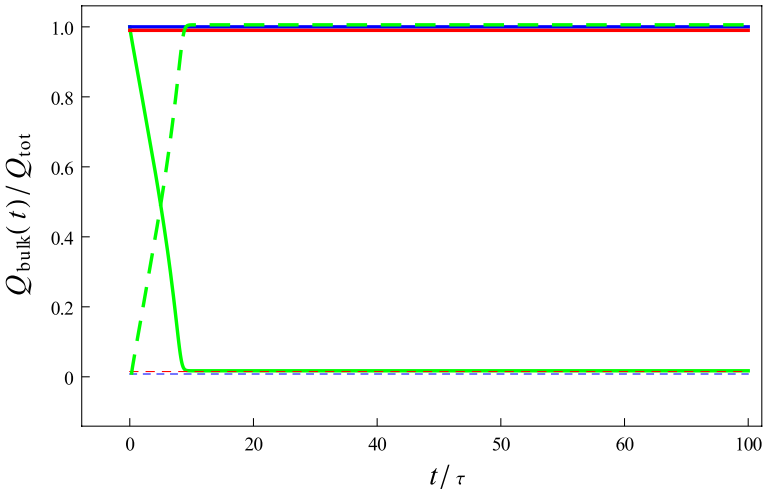

Fig. 7 Same systems as in Fig. 6 but now for the time dependence of the F-vortex charge in the bulk (full lines) and the vortex current flow through ther boundary (dashed lines). While the limit cycle (blue) and chaos (red) keep all vortex charge in the bulk, dissipation toward the trivial equilibrium (green) has a systematic vortex flow toward the edges. This is a finite-size effect which would not happen in an infinite field (but it does happen in real-world PR crystals which are, of course, finite)

The other curves in Fig. 4 describe dynamics which does not result in a nontrivial static pattern. The blue curve shows a limit cycle leading to periodic oscillations of the pattern, with half-period about 10τ. The corresponding patterns are seen in Fig. 6a, where we see how the vortex lattice keeps coming back to the original configuration at times $\approx 5\tau, 10\tau, 15\tau$. The red curve corresponds to the chaotic regime with aperiodic dynamics and no relaxation, as in Fig. 6b. Here the pattern keeps changing, wandering among the original lattice (for $t = 5\tau, 20\tau$), the inverse lattice (for $t = 10\tau$) and more or less incoherent patterns (for $t = 15\tau, 25\tau$). Finally, the green curve in Fig. 4 reaches a constant value of r. This corresponds to the pattern which radiates away in Fig. 6c, with total intensity being almost zero for $t > 20\tau$. Here one might wonder what happens to the vortex charge when the initially regular vortex lattice ends up as an incoherent, low-intensity configuration which obviously does not support vortices. The explanation is that the vortex charge flows outward, eventually reaching the edges of the crystal. The finite-size effects then invalidate the vortex charge conservation, as the usual proof that the winding number of the phase is a topological invariant crucially depends on considering the winding at infinity. Vortex charge thus dissipates at the edges. This is demonstrated in Fig. 7, which presents the same systems as in Fig. 6a–c but shows the ratio of the total bulk vortex charge $Q_{\rm bulk}(t)$ to the total initial vortex charge $Q_{\rm tot}$. Total initial charge is calculated by definition, as the integrated vorticity of the F-beam, $Q_{\rm tot} = \int dx \int dy |\boldsymbol{\omega}_F|$, with

$$\boldsymbol{\omega}_F = \left(\cos\theta_F \partial_x \theta_F, \sin\theta_F \partial_y \theta_F\right), \tag{11}$$

and all the quantities are taken at $t = 0$. The integral $\int dx \int dy |\boldsymbol{\omega}_F|$ equals precisely the total F-vortex charge summed over all vortices. The bulk charge is computed by subtracting the integrated vorticity flow along the boundary:

$$Q_{\rm bulk}(t) = Q_{\rm tot} - \int_0^t dt' \oint d\mathbf{l} \cdot \boldsymbol{\omega}_F(t). \tag{12}$$

Figure 7 shows that the sum of the bulk charge and the vortex current through the boundary is preserved in all cases, including when chaos or dissipation makes the pattern incoherent. In the last case, however, all the vortex charge flows toward the boundaries – this is a finite-size effect which would be absent in infinite field but is observable in realistic PR-crystals which are of finite dimensions. In practice, the matters are even more complicated as the boundary surface carries also new physics (surface polarization etc.), so the starting equations of motion would have to be modified. We believe, however, that the basic picture of vortex charge dissipating at the boundary still remains, because the mapping from the internal $U(1)$ phase onto the loop in the coordinate plane is explicitly broken by the boundary (whatever its detailed physics might be), and the vortex charge nonconservation at the boundary follows from this breaking.

The next task is to consider in more detail the decay of an ordered phase, either to chaos or to a limit cycle (radiating away all intensity is likely a trivial process, fully described by the approximately constant decay rate). We plan to address this problem in further work, and to relate the results to the question of quench dynamics in vortex systems.

Acknowledgements Work at the Institute of Physics is funded by Ministry of Education, Science and Technological Development, under Grants Nos. OI171033 and OI171017. M.P. is also supported by the NPRP 8-028-1-001 project of the Qatar National Research Fund (a member of the Qatar Foundation).

References

Alexander, T.J., Desyatnikov, A.S., Kivshar, Y.S.: Multivortex solitons in triangular photonic lattices. Opt. Lett. **32**, 1293–1295 (2007)

Anderson, P.W.: Two new vortex liquids. Nat. Phys. **3**, 160–162 (2007)

Antenucci, F., Conti, C., Crisanti, A., Leuzzi, L.: General phase diagram of multimodal ordered and disordered lasers in closed and open cavities. Phys. Rev. Lett. **114**, 043901 (2015a)

Antenucci, F., Crisanti, A., Leuzzi, L.: Complex spherical 2 + 4 spin glass: a model for nonlinear optics in random media. Phys. Rev. A **91**, 053816 (2015b)

Arnol'd, V.I., Afraymovich, V.S., Il'yashenko, Y.S., Shil'nikov, L.P.: Bifurcation Theory and Catastrophe Theory. Springer, Berlin (1994)

Bagnato, V.S., Frantzeskakis, D.J., Kevrekidis, P.G., Malomed, B.A., Mihalache, D.: Bose–Einstein condensation: twenty years after. Rom. Rep. Phys. **67**, 5–50 (2015)

Berezinsky, V.L.: Destruction of long range order in one-dimensional and two-dimensional systems having a continuous symmetry group. 1. Classical systems. Sov. Phys. JETP **32**, 493–500 (1971)

Cardy, J.L., Ostlund, S.: Random symmetry-breaking fields and the XY model. Phys. Rev. B **25**, 6899–6909 (1982)

Castellana, M., Parisi, G.: Non-petturbative effects in spin glasses. Nat. Sci. Rep. **5**, 8697 (2015). arXiv :1503.02103 [cond-mat.dis-nn]

Cohen, O., Lan, S., Harmon, T., Giordmaine, J.A., Segev, M.: Spatial vector solitons consisting of counterpropagating fields. Opt. Lett. **27**, 2013–2015 (2002)

Cross, M., Hohenberg, P.: Pattern formation outside of equilibrium. Rev. Mod. Phys. **65**, 851–1112 (1993)

Čubrović, M., Petrović, M.: Quantum criticality in photorefractive optics: vortices in laser beams and antiferromagnets. Phys. Rev. A **96**, 053824 (2017). arXiv:1701.03451 [physics.optics]

Denz, C., Schwab, M., Weilnau, C.: Transverse Pattern Formation in Photorefractive Optics. Springer, Berlin (2003)

Dreischuh, E., Chervenkov, S., Neshev, D., Paulus, G.G., Walther, H.: Generation of lattice structures of optical vortices. J. Opt. Soc. Am. B **19**, 550–556 (2002)

Fetter, A.L.: Rotating trapped Bose–Einstein condensates. Rev. Mod. Phys. **81**, 647–691 (2009)

Fleischer, J.W., Bartal, G., Cohen, O., Manela, O., Segev, M., Hudock, J., Christodoulides, D.N.: Observation of vortex-ring "discrete" solitons in 2D photonic lattices. Phys. Rev. Lett. **92**, 123904 (2004)

Ghofraniha, N.: Experimental evidence of replica symmetry breaking in random lasers. Nat. Commun. **6**, 6058 (2015). arxiv.org/abs/1407.5428 [cond-mat.dis-nn]

Jović, D.M., Petrović, M.S., Belić, M.R.: Counterpropagating pattern dynamics: from narrow to broad beams. Opt. Commun. **281**, 2291–2300 (2008)
Kosterlitz, J., Thouless, D.: The Kosterlitz–Thouless phase in a hierarchical model. J. Phys. C **6**, 1181–1203 (1973)
Ma, X., Driben, R., Malomed, B., Meoer, T., Schumacher, S.: Two-dimensional symbiotic solitons and vortices in binary condensates with attractive cross-species interaction. Nat. Sci. Rep. **6**, 34847 (2016). arXiv:1606.08579 [physics.optics]
Malomed, B., Torner, L., Wise, F., Mihalache, D.: On multidimensional solitons and their legacy in contemporary atomic, molecular and optical physics. J. Phys. B: At. Mol. Opt. Phys. **49**, 170502 (2016)
Neshev, D.N., Alexander, T.J., Ostrovskaya, E.A., Kivshar, Y.S.: Observation of discrete vortex solitons in opticlly induced photonic lattices. Phys. Rev. Lett **92**, 123903 (2004)
Perret, A., Ristivojevic, Z., Le Doussal, P., Schehr, G., Wiese, K.: Super-rough glassy phase of the random field XY model in two dimensions. Phys. Rev. Lett. **109**, 157205 (2012). arXiv:1204.5685 [cond-mat.dis-nn]
Petrović, M.S., Belić, M.R., Denz, C., Kivshar, YuS: Counterpropagating optical beams and solitons. Lasers Photonic Rev. **5**, 214–233 (2011). arXiv:0910.4700 [physics.optics]
Petrović, M., Jović, D., Belić, M., Schröder, J., Jander, P., Denz, C.: Two dimensional counterpropagating spatial solitons in photorefractive crystals. Phys. Rev. Lett **95**, 053901 (2005)
Rabinovich, M.I., Ezersky, A.B., Weidman, P.D.: The Dynamics of Patterns. World Scientific, Singapore (2000)
Rechtsman, M.C., Zeuner, J.M., Plotnik, Y., Lumer, Y., Podolsky, D., Dreisow, F., Nolte, S., Segev, M., Szameit, A.: Photonic Floquet topological insulators. Nature **496**, 196–200 (2013). arXiv:1212.3146 [physics]
Sandfuchs, O., Kaiser, F., Belić, M.R.: Self-organization and Fourier selection of optical patterns in a nonlinear photorefractive feedback system. Phys. Rev. A **64**, 063809 (2001)
Silaev, M., Babev, E.: Microscopic derivation of two-component Ginzburg–Landau model and conditions of ots applicability in two-band systems. Phys. Rev. B **85**, 134514 (2012). arXiv:1110.1593 [cond-mat.supr-con]
Terhalle, B., Richter, T., Desyatnikov, A.S., Neshev, D.N., Krolikowski, W., Kaiser, F., Denz, C., Kivshar, Y.S.: Observation of multivortex solitons in photonic lattices. Phys. Rev. Lett **101**, 013903 (2008)